Quantum metrology with an N-qubit W superposition state under noninteracting and interacting operations

Yan Li [1,2,*] and Zhihong Ren[3]

[1]*Department of Physics, Taiyuan Normal University, Jinzhong, 030619, China*
[2]*Institute of Computational and Applied Physics, Taiyuan Normal University, Jinzhong, 030619, China*
[3]*School of Physics and Information Engineering, Shanxi Normal University, Taiyuan, 030031, China*

(Received 30 August 2022; accepted 15 December 2022; published 3 January 2023)

We study the performance of an N-qubit W superposition state composed of a W state and its obverse in quantum metrology. Taking advantage of the general Ising-type Hamiltonian (including *noninteracting* and *interacting* operation), we analytically present the quantum Fisher information (QFI) of an N-qubit W superposition state under different situations and then investigate its phase sensitivity. The results show that the phase sensitivity under noninteracting operation displays a crossover from the W state to Greenberger-Horne-Zeilinger (GHZ) state, where it is same as W state in the few-qubit case ($N \leqslant 6$) but asymptotically equal to the GHZ state for large-qubit cases ($N \gg 1$). Interestingly, the 4-qubit W superposition state is found to have the same sensitivity as the 4-qubit GHZ state. And the optimal measurement protocols are provided for ideal metrology. Under the phase-amplitude damping channel, the phase sensitivity of the W superposition state (except for $N = 3$) is ultimately decreased to the standard quantum limit, while it turns worse in a depolarizing channel. Finally, the tunable phase sensitivity under interacting operation is studied, and the general Heisenberg limit is surpassed with the increasing interaction strength γ. Meanwhile, a plateau of QFI and phase sensitivity is found for all large-qubit W superposition states, which is similar to the study of the GHZ state and again verifies the common feature of GHZ-type states in quantum metrology.

DOI: 10.1103/PhysRevA.107.012403

I. INTRODUCTION

Quantum metrology, with quantum squeezing and quantum entanglement as the key resources, plays an important and fundamental role in measurement of physical parameters [1,2], including gravitational wave detection [3], magnetometry [4,5], atomic clock [6], and biological measurement [7], etc. A high-precision metrology scheme generally includes three stages: preparation of the probe state, evolution under different scenarios (or phase encoding), and probe readout [8]. As dictated by quantum Cramér-Rao bound (qCRB) in statistics [9,10], the phase sensitivity is limited by quantum Fisher information (QFI), which is theoretically decided by the probe state and Hamiltonian [11]. Many kinds of strategies have been proposed to realize high-resolution measurement from theory and experiment [1,12–17], and it mainly is divided into two categories, the classical state with nonlinear Hamiltonian and the nonclassical state with linear Hamiltonian. Specifically, the measurement limit is achieved from the separable state under the nonlinear Hamiltonian [18] and alternatively, the constructed maximal entangled state under the linear Hamiltonian [19,20]. Here we focus on the general nonclassical state under the nonlinear Hamiltonian [21,22].

Recently, the N-qubit W superposition state,

$$|W\bar{W}_N\rangle = \frac{1}{\sqrt{2}}(|W_N\rangle + |\bar{W}_N\rangle), \tag{1}$$

composed of the symmetric W state

$$|W_N\rangle = \frac{1}{\sqrt{N}}(|0^{\otimes(N-1)}\rangle|1\rangle + \sqrt{N-1}|W_{N-1}\rangle|0\rangle) \tag{2}$$

and its obverse $\bar{W}$

$$|\bar{W}_N\rangle = \frac{1}{\sqrt{N}}(|1^{\otimes(N-1)}\rangle|0\rangle + \sqrt{N-1}|\bar{W}_{N-1}\rangle|1\rangle), \tag{3}$$

has been studied in theory and experiment [23–27]. Although it belongs to the GHZ entanglement class, it behaves differently from the GHZ state in quantum information processing. For example, the GHZ state has only genuine three-party entanglement, whereas the W superposition state also possesses the pairwise entanglement and hence can be more robust to the loss of qubits [23]. How about its performance in quantum metrology—Does it perform better than the GHZ state or the W state?

In this work we pursue this question and present a detailed study of the N-qubit W superposition state from the perspective of quantum metrology. By utilizing QFI, we investigate the phase sensitivity of the N-qubit W superposition state under an Ising-type Hamiltonian [28,29]. We first present the analytical QFI of the N-qubit W superposition under noninteracting operation and analyze the phase sensitivity with respect to the number of qubits involved. The results show that the phase sensitivity is the same as the W state for the few-qubit case, whereas it is asymptotically equal to the GHZ state in the larger qubit case. Interestingly, the 4-qubit W superposition state is found to have the same QFI with the

*Corresponding author: li8989971@163.com

4-qubit GHZ state. Based on parity measurement [30,31], the specific measurement protocols for the ideal metrology limit are provided and verified. Subsequently, the phase sensitivity of an N-qubit W superposition state under three decoherence channels is studied. Except for the 3-qubit case, the phase sensitivity of the other superposition state is decreased to the standard quantum limit (SQL) in the phase-amplitude damping channel, while it turns worse in the depolarizing channel.

Considering the interference between nearby noninteracting operations on the large-qubit quantum state [32–35], we then explore the performance of an N-qubit W superposition state under the Ising-type interacting operation. With the increasing interaction strength γ, the phase sensitivity of all W superposition state surpasses the general Heisenberg limit. Taking the 3-qubit W superposition state as a paradigm, we compare the phase sensitivity with the W state and GHZ state, and it shows that the W superposition state performs a little worse than the others. In the study of the large-qubit case, a plateau of QFI and phase sensitivity with respect to γ is found, similar to the study of the GHZ state [22], which again verifies the common feature of GHZ-type quantum states in quantum metrology. With respect to the special case of a 4-qubit W superposition state, the QFI is still found to be the same as the 4-qubit GHZ state, which reveals the consistency of both in quantum metrology under either noninteracting operation or interacting operation.

The remainder of the paper is organized as follows. We start by reviewing the relationship between the quantum Cramér-Rao lower bound and QFI in Sec. II. In Sec. III we investigate the phase sensitivity of an N-qubit W superposition state under noninteracting operation. Additionally, we present the optimal measurement protocol with respect to the specific W superposition state and study the effect of decoherence channels on the precision limit. In Sec. IV we also study the phase sensitivity of the N-qubit W superposition state under Ising-type interacting operation and compare its performance with the W and GHZ state. Finally, the results are summarized in Sec. V.

II. MODEL AND METHOD

Let us take quantum interferometry as a platform to illustrate the relationship between the quantum Cramér-Rao bound and Fisher information. Given the general quantum resources (quantum state and systematic Hamiltonian), we briefly review the formula to access QFI under different circumstances, including the ideal situation and noisy environments. With respect to the simplest two-body Hamiltonian given by Ising-type interacting operation, we present the formula to acquire QFI ideally.

A. Quantum Cramér-Rao bound and Fisher information

Here we consider a general estimation problem of the unknown phase shift θ_0 in quantum interferometry. Given ν independent repeated experimental results $\varepsilon = \{\varepsilon_1, ..., \varepsilon_\nu\}$, we can theoretically obtain the likelihood function $p(\varepsilon|\theta_0)$ from the conditional probability $p(\varepsilon_i|\theta_0)$ that receiving the result ε_i conditioned on estimated phase θ_0. With respect to the unbiased estimation method (e.g., maximum likelihood estimation or Bayesian inference [36]), the smallest standard error of the estimator θ_{est} is limited by the Cramér-Rao bound,

$$\Delta\theta_{est} \geqslant \frac{1}{\sqrt{\nu F(\theta)}}. \tag{4}$$

Evidently, the phase sensitivity is bounded by the quantity $F(\theta)$, which is the Fisher information and formally defined by [37]

$$F(\theta) \equiv \sum_{\varepsilon_i} p(\varepsilon_i|\theta)\left(\frac{\partial \ln p(\varepsilon_i|\theta)}{\partial\theta}\right)^2, \tag{5}$$

and the larger the Fisher information, the better the phase sensitivity.

In quantum mechanics, for a unitary phase encoding denoted by $\hat{\rho}_\theta = e^{-i\theta\hat{H}}\hat{\rho}_0 e^{i\theta\hat{H}}$, the maximal Fisher information is given by quantum Fisher information [11],

$$F_Q[\hat{\rho}_0, \hat{H}] = 2\sum_{i,j=1}^{k}\frac{(\lambda_i-\lambda_j)^2}{\lambda_i+\lambda_j}|\langle\psi_i|\hat{H}|\psi_j\rangle|^2, \tag{6}$$

where the diagonalized density matrix $\hat{\rho}_0$ is expressed as $\hat{\rho}_0 = \sum_{i=1}^{k}\lambda_i|\psi_i\rangle\langle\psi_i|$, and $\hat{H}$ is the phase generator representing the Hamiltonian in the quantum system. For an ideal pure state $\hat{\rho}_0 = |\psi_{in}\rangle\langle\psi_{in}|$ in the quantum interferometer, Eq. (6) is reduced to

$$F_Q = 4\Delta^2\hat{H}, \tag{7}$$

where $\Delta^2\hat{H} = \langle\hat{H}^2\rangle - \langle\hat{H}\rangle^2$. Therefore, the quantum Cramér-Rao bound becomes

$$\Delta\theta_{est} \geqslant \frac{1}{\sqrt{\nu F_Q}}, \tag{8}$$

and the key point in quantum metrology is the access of QFI from the given quantum system [38–42].

B. Quantum Fisher information under the Ising-type interacting operation

In the field of quantum many-body interactions, the simplest and well-known interaction model is the Ising-type interacting operation, such as nearest-neighbor coupling and fully connected coupling. It is generally given by [43]

$$\hat{H} = \hat{H}_0 + \hat{H}_1, \tag{9}$$

where $\hat{H}_0 = \sum_{i=1}^{N}\frac{\mu_i}{2}\sigma_m^{(i)}$ and $\hat{H}_1 = \sum_{i,j=1}^{N}\frac{V_{ij}}{4}\sigma_n^{(i)}\sigma_n^{(j)}$ denote the noninteracting operation and interacting operation, respectively. Here μ_i means the inhomogeneous linear couplings, and $V_{ij} = V_{ji}$, $\sigma_n^{(i)} = \sigma^{(i)}\cdot\vec{n}$ is the Pauli matrix for the ith particle and $\vec{n}$ is a vector.

According to the formula of QFI for the pure state, Eq. (7), we have

$$F_Q = v_0^2 + v_1^2 + v_2^2, \tag{10}$$

in which $v_0^2 = 4\Delta^2\hat{H}_0$, $v_1^2 = 4\Delta^2\hat{H}_1$, and $v_2^2 = 4(\langle\{\hat{H}_0, \hat{H}_1\}\rangle - 2\langle\hat{H}_0\rangle\langle\hat{H}_1\rangle)$ separately represent the noninteracting QFI, interacting QFI, and covariant QFI. With respect to a general

quantum state and two-body interacting operation, Eq. (9), the QFI is obtained by

$$v_0^2 = \sum_{i=1}^{N} \mu_i^2 \left(1 - \langle \sigma_m^{(i)} \rangle^2\right) + \sum_{\substack{i,j=1 \\ i\neq j}}^{N} \mu_i \mu_j \left(\langle \sigma_m^{(i)} \sigma_m^{(j)} \rangle - \langle \sigma_m^{(i)} \rangle \langle \sigma_m^{(j)} \rangle\right), \tag{11}$$

$$v_1^2 = \sum_{\substack{i,j=1 \\ i\neq j}}^{N} \frac{V_{ij}^2}{2} \left(1 - \langle \sigma_n^{(i)} \sigma_n^{(j)} \rangle^2\right) + \sum_{\substack{i,j,k=1 \\ i\neq j\neq k}}^{N} V_{ij} V_{jk} \left(\langle \sigma_n^{(i)} \sigma_n^{(k)} \rangle - \langle \sigma_n^{(i)} \sigma_n^{(j)} \rangle \langle \sigma_n^{(j)} \sigma_n^{(k)} \rangle\right) + \sum_{\substack{i,j,k,l=1 \\ i\neq j\neq k\neq l}}^{N} \frac{V_{ij} V_{kl}}{4} \left(\langle \sigma_n^{(i)} \sigma_n^{(j)} \sigma_n^{(k)} \sigma_n^{(l)} \rangle - \langle \sigma_n^{(i)} \sigma_n^{(j)} \rangle \langle \sigma_n^{(k)} \sigma_n^{(l)} \rangle\right), \tag{12}$$

$$v_2^2 = 2 \sum_{\substack{i,j=1 \\ i\neq j}}^{N} \mu_i V_{ij} \left(\mathbf{m} \cdot \mathbf{n} \langle \sigma_n^{(j)} \rangle - \langle \sigma_n^{(i)} \sigma_n^{(j)} \rangle \langle \sigma_m^{(i)} \rangle\right) + \sum_{\substack{i,j,k=1 \\ i\neq j\neq k}}^{N} \mu_k V_{ij} \left(\langle \sigma_n^{(i)} \sigma_n^{(j)} \sigma_m^{(k)} \rangle - \langle \sigma_n^{(i)} \sigma_n^{(j)} \rangle \langle \sigma_m^{(k)} \rangle\right). \tag{13}$$

In light of the permutation symmetry of the N-qubit W superposition state, the calculation of QFI mainly focuses on the expectation value of interactive qubits, i.e., $\langle \sigma_n^{(i)} \rangle$, $\langle \sigma_n^{(i)} \sigma_n^{(j)} \rangle$, and $\langle \sigma_n^{(i)} \sigma_n^{(j)} \sigma_n^{(k)} \sigma_n^{(l)} \rangle$. Next we will exploit the above formulas to present the specified QFI with respect to the given W superposition state and further analyze its phase sensitivity.

III. METROLOGY LIMIT OF N-QUBIT W SUPERPOSITION STATE UNDER NONINTERACTING OPERATION

In order to fully understand the performance of the N-qubit W superposition state in quantum metrology, we first investigate the traditional metrology limit of the N-qubit W superposition state from the point of noninteracting operation, then present the corresponding measurement protocols, and at last the effect of decoherence channels on the metrology limit is considered.

A. Ideal metrology limit of the N-qubit W superposition state under noninteracting operation

We begin with the noninteracting operation (collective generator $\hat{H}_0$, $\mu_i = 1\ \forall i$) and investigate the phase sensitivity of the N-qubit W superposition state by QFI. Assuming $\sigma_m^{(i)} = a\sigma_x^{(i)} + b\sigma_y^{(i)} + c\sigma_z^{(i)}$ and $a^2 + b^2 + c^2 = 1$, the expectation value of the specified interactive terms in Eq. (11) is calculated as

$$\langle \sigma_m^{(i)} \rangle = \begin{cases} \frac{2a}{3}, & N = 3 \\ 0, & N \neq 3 \end{cases} \tag{14}$$

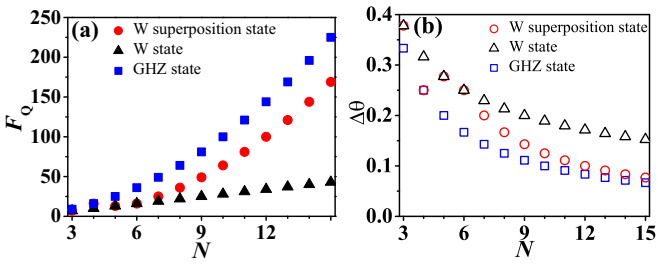

FIG. 1. QFI and phase sensitivity with respect to the number of qubits N under noninteracting operation. (a) Red dots, black triangles, and blue squares respectively denote the QFI of an N-qubit W superposition state, W state, GHZ state. (b) Red circles, black hollow triangles, and blue hollow squares represent the corresponding phase sensitivity, separately.

and

$$\langle \sigma_m^{(i)} \sigma_m^{(j)} \rangle = \begin{cases} a^2, & N = 4 \\ \frac{2+(N-6)c^2}{N}, & N \neq 4 \end{cases}. \tag{15}$$

Therefore the optimized noninteracting QFI of an N-qubit W superposition state (except for $N = 4$) is obtained and represented by

$$F_Q^{(N)} = 3N - 2 + (N-1)(N-6)c^2. \tag{16}$$

The 4-qubit W superposition state is a special case, and its noninteracting QFI is written as

$$F_Q^{(4)} = 4 + 12a^2. \tag{17}$$

To vividly exhibit the feature of the N-qubit W superposition state in quantum metrology, we show the optimized noninteracting QFI (red dots) and phase sensitivity $\Delta\theta$ (red circles) with respect to the number of qubits N in Fig. 1. As a comparison, we have also added the results of the N-qubit W state (triangles) and N-qubit GHZ state (squares).

Obviously, when the number of qubits N is smaller than 6, the noninteracting QFI and phase sensitivity $\Delta\theta$ of the W superposition state are the same as the W state and behave as a feature of the W state, i.e., Eq. (16) for $N \leqslant 6$. With the increasing number of qubits ($N \geqslant 7$), the noninteracting QFI becomes

$$F_Q^{(N)} = (N-2)^2, \tag{18}$$

which is asymptotically equal to the QFI of the GHZ state for larger N, $F_Q^{(\mathrm{GHZ})} = N^2$, and displays the features of the GHZ state. During the middle region in Fig. 1(b), the phase sensitivity (red circles) shows a crossover from the W state (black hollow triangles) to the GHZ state (blue hollow squares).

Specially, we have found that the optimized QFI of a 4-qubit W superposition state is $F_Q^{(4)} = 16$, which indicates the same sensitivity with the 4-qubit GHZ state. Moreover, from Ref. [23] we know the W superposition state behaves more robustly to the loss of qubits than the GHZ state, which may shed some new light on high-precision metrology, especially in relatively noisy environments. It is also possible to replace the 4-qubit GHZ state with it to manage some quantum computational tasks [44]. Besides, from the point of view of entanglement detection and classification [45–47], it

also raises the dilemma that we cannot distinguish both via noninteracting QFI.

B. Optimal measurement protocols for *N*-qubit *W* superposition state

In this section the optimal measurement protocols of the N-qubit W superposition state for the ideal metrology limit are presented. As is well known, the parity measurement has been adopted to realize the optimal metrology in many experiments [31], such as the optical Mach-Zehnder (M-Z) interferometry [48] and others [49,50]. Combined with the similarity of the W superposition state and GHZ state in the study of phase sensitivity, we here employ parity measurement to explore the optimal metrology scheme. The general form of parity operator in the qubit system is expressed as [51]

$$\hat{\Pi}(\alpha,\beta)=\bigotimes_{i=1}^{N}(\hat{\sigma}\cdot\vec{n})^{(i)}, \tag{19}$$

and the eigenvalues are $\varepsilon_+=+1$ and $\varepsilon_-=-1$. The specific ones can be reduced by the choice of vector $\vec{n}=(\sin\alpha\cos\beta,\sin\alpha\sin\beta,\cos\alpha)$, e.g., the analysis operator $\hat{\Pi}(\pi/2,\beta)$ for witnessing the GHZ state [52].

The standard procedures referring to the probe state in M-Z interferometry include three parts: the initial state preparation, evolution or phase shift encoding, and measurement for higher precision metrology. Actually, the preparation of a 3-qubit W superposition state has been realized in experimentation [25], and what we need to do is to find an optimal strategy to reach the ideal metrology limit, that is, to perfectly complete the last two steps. The evolution of a general W superposition state is depicted by the operator $e^{-i\hat{J}_m\theta}$, where $\hat{J}_m=\frac{1}{2}\sum_{i=1}^{N}\hat{\sigma}_m$ $(m=x,y,z)$ denotes the collective angular momentum operator, and the measured physical quantity is the parity operator mentioned previously. In the following we will explicitly present the optimal scheme for every N-qubit W superposition state. Similar to the previous section, it is divided into four categories, including the 3-qubit W superposition state, the 4-qubit W superposition state, the 5,6-qubit W superposition state, and the N-qubit case.

In the case of the 3-qubit W superposition state, we numerically calculate and find the optimal strategy where the output density matrix is expressed as

$$\hat{\rho}_\theta=e^{-i\hat{J}_y\theta}\hat{\rho}_0e^{i\hat{J}_y\theta}, \tag{20}$$

and $\hat{\rho}_0=|W\bar{W}_3\rangle\langle W\bar{W}_3|$ denotes the initial probe state. The measured parity operator is given by $\hat{\Pi}(\pi/2,0)$, and so the averaged value is accessed by

$$\begin{aligned}\langle\hat{\Pi}\rangle&=\mathrm{Tr}[\hat{\rho}_\theta\hat{\Pi}(\pi/2,0)]=\mathrm{p}_3(\varepsilon_+|\theta)-\mathrm{p}_3(\varepsilon_-|\theta)\\&=\tfrac{1}{4}(\cos\theta+3\cos3\theta).\end{aligned} \tag{21}$$

Combined with the relationship $p_3(\varepsilon_+|\theta)+p_3(\varepsilon_-|\theta)=1$, the conditional probability $p_3(\varepsilon_+|\theta)$ is obtained,

$$p_3(\varepsilon_+|\theta)=\tfrac{1}{2}+\tfrac{1}{8}(\cos\theta+3\cos3\theta). \tag{22}$$

Substituting Eq. (22) into the formula of Fisher information, Eq. (5), we have

$$F^{(3)}(\theta)=\frac{\csc^2\theta(\sin\theta+9\sin3\theta)^2}{2(23+24\cos2\theta+9\cos4\theta)}, \tag{23}$$

and by maximizing it, the QFI $F_Q^{(3)}=7$ is obtained at the optimal phase shift $\theta_{\mathrm{op}}^{(3)}=k\cdot2\pi$ $(k=0,1,2...)$. This means that the ideal metrology limit can be theoretically realized with Eq. (8).

With respect to the special case, the 4-qubit W superposition state, the optimal scheme is realized through the rotation operator $e^{-i\hat{J}_x\theta}$ acting on the probe state. Similarly, the measured parity operator is numerically obtained and shown as $\hat{\Pi}(0,\pi/2)$. Therefore the conditional probability is obtained and given by

$$p_4(\varepsilon_+|\theta)=\tfrac{1}{2}(1-\cos4\theta). \tag{24}$$

Fisher information $F^{(4)}(\theta)=16$ is easily obtained by replacing Eq. (24) into Eq. (5). It is evident that $F^{(4)}(\theta)$ is equal to $F_Q^{(4)}$, which implies that the ideal metrology limit can be achieved in all of the phase shift region.

For the 5,6-qubit W superposition state, the optimal strategies are the same as the 3-qubit case and are realized by the rotation operator $e^{-i\hat{J}_y\theta}$ and measured parity operator $\hat{\Pi}(\pi/2,0)$. In brief, the conditional probabilities are respectively shown by

$$p_5(\varepsilon_+|\theta)=\tfrac{1}{2}+\tfrac{1}{4}\cos\theta^3(5\cos2\theta-3) \tag{25}$$

and

$$p_6(\varepsilon_+|\theta)=\tfrac{1}{2}+\tfrac{1}{16}(5\cos2\theta+3\cos6\theta). \tag{26}$$

The QFI can be obtained in the same way, and the optimal phase shifts for the ideal metrology limit are $\theta_{\mathrm{op}}^{(5)}=k\cdot2\pi$ $(k=0,1,2...)$ and $\theta_{\mathrm{op}}^{(6)}=k\cdot\pi$ $(k=0,1,2...)$.

As the number of qubits involved is larger than 6, we find that the optimal strategies of the N-qubit W superposition state are the same and depicted by the rotation operator $e^{-i\hat{J}_z\theta}$ and measured parity operator $\hat{\Pi}(\pi/2,0)$. Therefore the conditional probability is represented as

$$p_N(\varepsilon_+|\theta)=\tfrac{1}{2}[1-\cos(N-2)\theta], \tag{27}$$

and substituting it into Eq. (5), we obtain the Fisher information $F^{(N)}(\theta)=(N-2)^2$, equaling QFI. This implies that the ideal metrology limit of the N-qubit W superposition state can be obtained in all of the phase shift region. Besides, the conditional probability Eq. (27) is very similar to the GHZ state [53] and reflects the consistency of both, to some extent.

C. Decoherence effects on the ideal metrology limit

Decoherence exists in all physical systems, and in this section we study the phase sensitivity of the N-qubit W superposition state under three decoherence channels [54], i.e., depolarizing, phase damping, and amplitude damping. The Kraus representation used to describe the density matrix after decoherence is generally given by [55]

$$K(\hat{\rho})=\sum_k\hat{E}_k\hat{\rho}\hat{E}_k^\dagger, \tag{28}$$

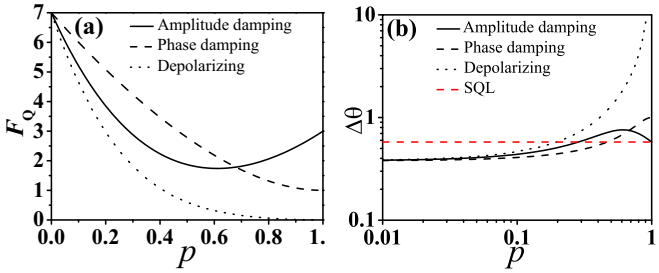

FIG. 2. QFI and phase sensitivity of 3-qubit W superposition state under decoherence channels. (a) The QFI with respect to p under a depolarizing channel (dot line), phase damping channel (dash line), and amplitude damping channel (solid line). (b) Similar to (a) but for the corresponding phase sensitivity, and the dashed red line denotes the SQL.

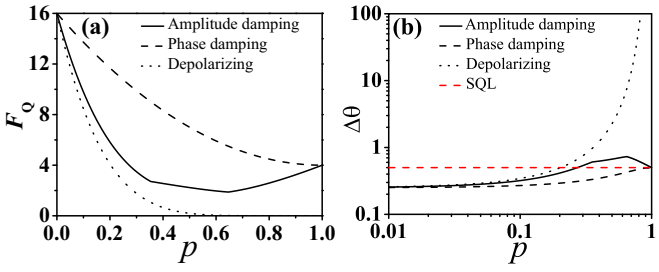

FIG. 3. QFI and phase sensitivity of 4-qubit W superposition state under decoherence channels. (a) The QFI with respect to p under a depolarizing channel (dot line), phase damping channel (dash line), and amplitude damping channel (solid line). (b) The corresponding phase sensitivities are shown, and the dashed red line represents the SQL.

where $\hat{E}_k$ denotes the Kraus operator and satisfies the completeness relationship

$$\sum_k \hat{E}_k^\dagger \hat{E}_k = \mathbf{1}. \tag{29}$$

According to the evolution of density matrix under different channels, the decohered density matrix of the N-qubit W superposition state is given by

$$K(\hat{\rho}) = \sum_{k_1,k_2,\ldots,k_N} (\hat{E}_{k_1} \otimes \hat{E}_{k_2} \otimes \cdots \otimes \hat{E}_{k_N}) \times \hat{\rho}(\hat{E}_{k_1} \otimes \hat{E}_{k_2} \otimes \cdots \otimes \hat{E}_{k_N})^\dagger. \tag{30}$$

Then we diagonalize it and substitute the eigenvalues and eigenvectors into Eq. (6) with $\hat{H}_0$ and $\mu_i = 1$, and therefore the decohered QFI of the N-qubit W superposition state is obtained. Finally, after maximizing QFI over all direction $\vec{n}$, the maximal QFI is achieved. Below we adopt the above procedures and take the 3,4-qubit W superposition state as paradigms to study the effect of three decoherence channels on the metrology limit.

1. Depolarizing

We first analyze the effect of the depolarizing channel with the Kraus operators:

$$\hat{E}_0 = \sqrt{1-\frac{3}{4}p}\mathbf{1}, \hat{E}_1 = \sqrt{\frac{p}{4}}\hat{\sigma}_x, \hat{E}_2 = \sqrt{\frac{p}{4}}\hat{\sigma}_y, \hat{E}_3 = \sqrt{\frac{p}{4}}\hat{\sigma}_z, \tag{31}$$

where p is the depolarizing coefficient. With respect to the state $|W\bar{W}_3\rangle$, the decohered density matrix is obtained by

$$K(\hat{\rho}_{W\bar{W}_3}) = \sum_{k_1,k_2,k_3=0}^{3} (\hat{E}_{k_1} \otimes \hat{E}_{k_2} \otimes \hat{E}_{k_3})|W\bar{W}_3\rangle\langle W\bar{W}_3| \times (\hat{E}_{k_1} \otimes \hat{E}_{k_2} \otimes \hat{E}_{k_3})^\dagger. \tag{32}$$

After diagonalization we obtain the eigenvalues and normalized eigenvectors, which are lengthy and not shown here. Substituting both into Eq. (10) and maximizing it over all directions $\vec{n} = (\sin\theta\cos\phi, \sin\theta\sin\phi, \cos\theta)$, the maximal QFI is acquired.

In the case of the 3-qubit W superposition state, the expression of QFI under a depolarizing channel is tedious and not shown. For the 4-qubit case, it is written as

$$F_Q^{de_4} = \frac{128(1-p)^8}{8-16p+12p^2-4p^3+p^4}. \tag{33}$$

In Figs. 2(a) and 3(a), the dotted lines depict the decohered QFI of a 3,4-qubit W superposition state with respect to p in the depolarizing channel, which reflects that the phase sensitivity becomes worse for larger p, see Figs. 2(b) and 3(b) for details.

2. Phase damping and amplitude damping

In the phase damping channel and amplitude damping channel, the Kraus operators are described by

$$\hat{E}_0 = \begin{pmatrix} \sqrt{1-p} & 0 \\ 0 & \sqrt{1-p} \end{pmatrix}, \hat{E}_1 = \begin{pmatrix} 0 & 0 \\ 0 & \sqrt{p} \end{pmatrix}, \hat{E}_2 = \begin{pmatrix} \sqrt{p} & 0 \\ 0 & 0 \end{pmatrix}, \tag{34}$$

and

$$\hat{E}_0 = \begin{pmatrix} 1 & 0 \\ 0 & \sqrt{1-p} \end{pmatrix}, \hat{E}_1 = \begin{pmatrix} 0 & \sqrt{p} \\ 0 & 0 \end{pmatrix}. \tag{35}$$

Taking advantage of the same procedures in the depolarizing channel, we obtain the decohered QFI of the 3-qubit and 4-qubit W superposition state under the phase damping channel,

$$F_Q^{pd_3} = \frac{126-354p+397p^2-204p^3+31p^4+12p^5-2p^6}{18-24p+12p^2} \tag{36}$$

and

$$F_Q^{pd_4} = 16-24p+12p^2, \tag{37}$$

which are shown by dashed lines in Figs. 2(a) and 3(a). Obviously, the decohered QFI of a 3-qubit W superposition state displays a different behavior from the result of the 4-qubit case, especially at the point of $p = 1$. Similarly, the corresponding phase sensitivity $\Delta\theta$ obtained by Eq. (8) is also different, as it is shown by dashed lines in Figs. 2(b) and 3(b). In the amplitude damping channel, the expressions of QFI ($F_Q^{ad_3}$ and $F_Q^{ad_4}$) for the 3-qubit W superposition state

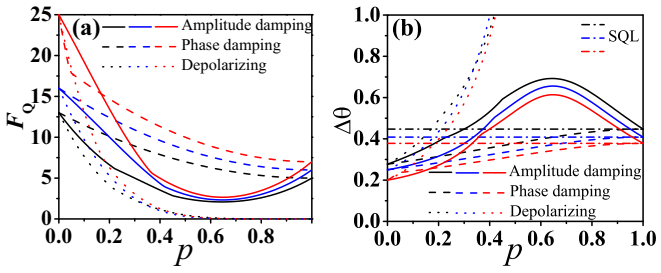

FIG. 4. QFI and phase sensitivity of 5,6,7-qubit W superposition states under decoherence channels. (a) From bottom to top, black, blue, and red lines respectively denote the QFI of a 5,6,7-qubit W superposition state with respect to p under a depolarizing channel (dot line), phase damping channel (dash line), and amplitude damping channel (solid line). (b) The corresponding phase sensitivities, from top (black) to bottom (red), with respect to p are shown, and the corresponding dashed dot lines represent the SQL.

and 4-qubit W superposition state are lengthy and not shown. We present the results in Figs. 2 and 3, where the solid lines denote the decohered QFI and corresponding phase sensitivity $\Delta\theta$ with respect to p, respectively. It is obvious that with increasing p the phase sensitivity is finally decreased to the SQL, but not so in the middle region. In addition, the values of $F_Q^{ad_N}$ for special p can be easily obtained, such as $p = 0$ (or $p = 1$), for which the decohered QFI is equal to Eq. (16) (or N). It is same in the phase damping channel except for the 3-qubit case, which can also be drawn from Fig. 4(a).

For comparison, we have also presented the decohered QFI and phase sensitivity of the $N = 5, 6, 7$-qubit W superposition states in Fig. 4. The results show that the phase sensitivity of the N-qubit W superposition state is always better than SQL in the phase damping channel, but not so in the amplitude damping channel and depolarizing channel.

IV. METROLOGY LIMIT OF N-QUBIT W SUPERPOSITION STATE UNDER INTERACTING OPERATION

This section we preliminarily explore the effect of interacting operation on the metrology limit. The nearest-neighbor Ising-type interacting operation ($V_{ij} = \gamma \frac{\delta_{j,i+1}+\delta_{j,i-1}}{2}$) is chosen as a prototype to investigate the phase sensitivity of the N-qubit W superposition state. Due to permutation symmetry of the given quantum state, the QFI is obtained only through the calculation of the expectation value in Eq. (10). Without loss of generality, it assumes $\mathbf{m}\cdot\mathbf{n} = 1$, $\mu_i = 1\ \forall i$, $\sigma_m^{(i)} = \sigma_n^{(i)} = a\sigma_x^{(i)} + b\sigma_y^{(i)} + c\sigma_z^{(i)}$, and $a^2 + b^2 + c^2 = 1$ as follows.

In the case of the 3-qubit W superposition state, the QFI is calculated and represented by

$$F_Q^{(3)} = 7 - 4a^2 - 6c^2 + 3a(1 - c^2)\gamma + \tfrac{3}{4}(1 + 2c^2 - 3c^4)\gamma^2, \tag{38}$$

and evidently the maximal QFI [maximizing Eq. (38) over the direction $\vec{n}$] is varied with interaction strength γ. In Fig. 5 we plot the maximal QFI and phase sensitivity $\Delta\theta$ with respect to γ, and meanwhile, the results of the W state and GHZ state are chosen for comparison [22]. It is shown that they all surpass the general Heisenberg limit with increasing γ, but the W superposition state performs a little worse than the others.

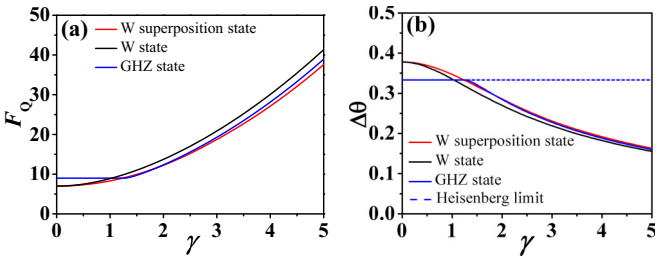

FIG. 5. QFI and phase sensitivity of 3-qubit W superposition state under interacting operation. (a) Red, blue, and black lines, from bottom to top (right-hand side), respectively denote the QFI of W superposition state, GHZ state, and W state with respect to interaction strength γ. (b) The corresponding phase sensitivity $\Delta\theta$ with respect to γ, and the dashed blue line denotes the general Heisenberg limit.

For the 4-qubit W superposition state, the QFI is written as

$$F_Q^{(4)} = 4(4a^2 + b^2 + c^2) + 4[2b^2c^2 + a^2(b^2 + c^2)]\gamma^2, \tag{39}$$

and after maximization it is reduced to

$$F_Q^{(4)} = \begin{cases} 16, & \gamma \leqslant \sqrt{3} \\ 2(2 + \frac{9}{\gamma^2} + \gamma^2), & \gamma \geqslant \sqrt{3} \end{cases}. \tag{40}$$

In Fig. 6 we show the QFI and phase sensitivity of a 4-qubit W superposition state with respect to γ (red lines), accompanied with the results from the 4-qubit GHZ state (blue lines) and 4-qubit W state (black lines). It is found that the plots of the 4-qubit W superposition state are exactly overlapped with the results of the 4-qubit GHZ state [22]. This is very interesting, that both perform consistently in quantum metrology, whether the noninteracting operation or interacting operation, and it may exhibit superiority in high-precision measurement and other related assignments.

We then have managed the case of 5,6-qubit W superposition states and separately presented the QFI as

$$F_Q^{(5)} = 13a^2 + 13b^2 + 9c^2 + 6a(a^2 - 3b^2)\gamma + \tfrac{1}{4}(a^2 + b^2)[5(a^2 + b^2) + 36c^2]\gamma^2 \tag{41}$$

and

$$F_Q^{(6)} = 16 + 3[(a^2 - b^2)^2 + 4(a^2 + b^2)c^2]\gamma^2. \tag{42}$$

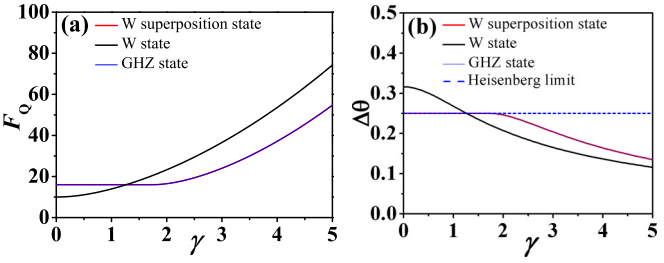

FIG. 6. QFI and phase sensitivity of a 4-qubit W superposition state under interacting operation. (a) Red, blue, and black lines, from bottom to top (right-hand side), respectively denote the QFI of a W superposition state, GHZ state, and W state with respect to interaction strength γ. (b) The corresponding phase sensitivity $\Delta\theta$ with respect to γ, and dashed blue line denotes the general Heisenberg limit.

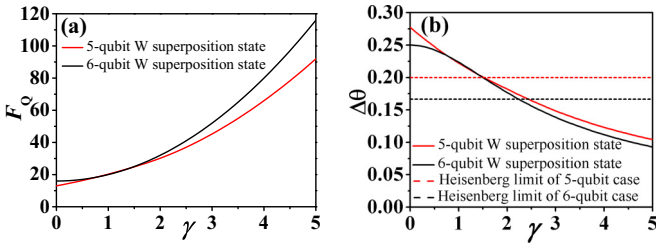

FIG. 7. QFI and phase sensitivity of 5-, 6-qubit W superposition states under interacting operation. (a) Red and black lines, from bottom to top, respectively denote the QFI of 5- and 6-qubit W superposition states with respect to interaction strength γ. (b) The solid and dashed lines, from top to bottom, represent the corresponding phase sensitivities and the general Heisenberg limits.

In Fig. 7 we show the QFI and phase sensitivity of 5,6-qubit W superposition states with respect to γ. It is found that there are two intersections from the results of a 5,6-qubit W superposition state. Besides, with increasing γ the general Heisenberg limit is also surpassed in both cases.

As the number of qubits involved is larger than 6, the formula of QFI of an N-qubit W superposition state is found and expressed by

$$F_Q^{(N)} = 3N - 2 + (N-1)(N-6)c^2 + \tfrac{1}{4}(1-c^2)(N+11Nc^2-24c^2)\gamma^2, \tag{43}$$

and by maximizing it we analytically obtain the optimal QFI,

$$F_Q^{(N)} = \begin{cases} (N-2)^2, & \gamma \leqslant \gamma_t \\ \frac{(N^2-7N+6)^2+(N-2)(5N^2-4N+12)\gamma^2+9(N-2)^2\gamma^4}{(11N-24)\gamma^2}, & \gamma \geqslant \gamma_t \end{cases}. \tag{44}$$

In Fig. 8 the QFI and phase sensitivity of 7-, 8-, 9-, 10-, 11-, and 12-qubit W superposition states with respect to γ are shown. A plateau is found for every W superposition state, and the turning point is analytically

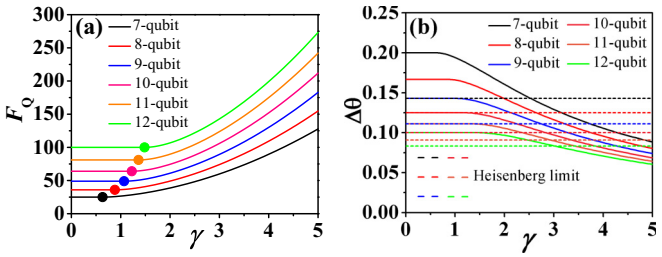

FIG. 8. QFI and phase sensitivity of 7-, 8-, 9-, 10-, 11-, and 12-qubit W superposition states under interacting operation. (a) Colorful lines, from bottom to top, respectively denote the QFI of 7-, 8-, 9-, 10-, 11-, and 12-qubit W superposition states with respect to interaction strength γ, and colorful dots represent the turning points given by Eq. (45). (b) The colorful solid and dashed lines, from top to bottom, represent the corresponding phase sensitivities and the general Heisenberg limits.

obtained and given by

$$\gamma_t = \sqrt{\frac{(N-6)(N-1)}{3(N-2)}}. \tag{45}$$

Obviously, it is approximately $\sqrt{N/3-2}$ for larger N, which is reminiscent of the plateau that emerged in the study of the GHZ state, where it is $\sqrt{N-1}$ [22]. This again implies the common feature of GHZ-type quantum states in quantum metrology.

V. CONCLUSIONS

In summary, we have analyzed the phase sensitivity of an N-qubit W superposition state under noninteracting and interacting operation by QFI. As presented in noninteracting operation, the phase sensitivity of an N-qubit W superposition state is the same as the W state for the number of qubits $N \leqslant 6$ and asymptotically equal to the GHZ state for larger qubits involved ($N \gg 1$). Interestingly, the 4-qubit W superposition state is found to have the same phase sensitivity as a 4-qubit GHZ state. This may shed some new light on high-precision metrology, especially in some relatively noisy environments. Based on parity measurement, we have presented the optimal measurement protocols for the ideal metrology limit with respect to every W superposition state. Considering the effect of decoherence on the metrology limit, we have shown the phase sensitivity of an N-qubit W superposition state with respect to p under different channels and found that it is always better than the standard quantum limit in the phase damping channel (except for the 3-qubit case). Finally, the phase sensitivity under Ising-type interacting operation was studied and the general Heisenberg limit is surpassed with increasing interaction strength γ for all W superposition states. In the case of a larger qubit W superposition state, a plateau of QFI and phase sensitivity with respect to γ is found, similar to the result of a GHZ state, which again verifies the common feature of GHZ-type quantum states in quantum metrology.

In addition, the phase sensitivity of a 4-qubit W superposition state is found to be the same as a 4-qubit GHZ state, whether under noninteracting operation or interacting operation. This deserves to be explored and may exhibit superiority in related topics. Meanwhile, it also raises a question regarding the aspect of entanglement detection and classification, that we cannot distinguish them via QFI, and this issue will be studied elsewhere.

ACKNOWLEDGMENTS

This work was supported by the National Natural Science Foundation of China (Grant No. 12205176), the Applied Basic Research Program of Shanxi Province (Grants No. 202203021212193 and No. 202103021223251), and the Scientific and Technological Innovation Programs of Higher Education Institutions in Shanxi (Grant No. 2020L0512).

[1] L. Pezzé, A. Smerzi, M. K. Oberthaler, R. Schmied, and P. Treutlein, Non-classical states of atomic ensembles: Fundamentals and applications in quantum metrology, Rev. Mod. Phys. **90**, 035005 (2018).

[2] Z. H. Ren, Y. Li, Y. N. Li, and W. D. Li, Development on quantum metrology with quantum Fisher information, Acta Phys. Sin. **68**, 040601 (2019).

[3] R. Schnabel, N. Mavalvala, D. E. McClelland, and P. K. Lam, Quantum metrology for gravitational wave astronomy, Nat. Commun. **1**, 121 (2010).

[4] J. B. Brask, R. Chaves, and J. Kołodyński, Improved Quantum Magnetometry beyond the Standard Quantum Limit, Phys. Rev. X **5**, 031010 (2015).

[5] Z. Hou, Z. Zhang, G. Y. Xiang, C. F. Li, G. C. Guo, H. Chen, L. Liu, and H. Yuan, Minimal Tradeoff and Ultimate Precision Limit of Multiparameter Quantum Magnetometry under the Parallel Scheme, Phys. Rev. Lett. **125**, 020501 (2020).

[6] L. Pezzé and A. Smerzi, Heisenberg-Limited Noisy Atomic Clock Using a Hybrid Coherent and Squeezed State Protocol, Phys. Rev. Lett. **125**, 210503 (2020).

[7] M. A. Taylor and W. P. Bowen, Quantum metrology and its application in biology, Phys. Rep. **615**, 1 (2016).

[8] V. Giovannetti, S. Lloyd, and L. Maccone, Quantum Metrology, Phys. Rev. Lett. **96**, 010401 (2006).

[9] C. W. Helstrom, *Quantum Detection and Estimation Theory* (Academic Press, New York, 1976).

[10] A. S. Holevo, *Probabilistic and Statistical Aspects of Quantum Theory* (North-Holland, Amsterdam, 1982).

[11] S. L. Braunstein and C. M. Caves, Statistical Distance and the Geometry of Quantum States, Phys. Rev. Lett. **72**, 3439 (1994).

[12] G. Tóth and I. Apellaniz, Quantum metrology from a quantum information science perspective, J. Phys. A: Math. Theor. **47**, 424006 (2014).

[13] H. Huo, M. Zhuang, J. Huang, and C. H. Lee, Machine optimized quantum metrology of concurrent entanglement generation and sensing, Quantum Sci. Technol. **7**, 025010 (2022).

[14] J. Yang, S. S. Pang, A. Campo, and A. N. Jordan, Super-Heisenberg scaling in Hamiltonian parameter estimation in the long-range Kitaev chain, Phys. Rev. Res. **4**, 013133 (2022).

[15] Y. Kim, S. Y. Yoo, and Y. H. Kim, Heisenberg-Limited Metrology via Weak-Value Amplification without Using Entangled Resources, Phys. Rev. Lett. **128**, 040503 (2022).

[16] Q. Liu, L. N. Wu, J. H. Cao, T. W. Mao, X. W. Li, S. F. Guo, M. K. Tey, and L. You, Nonlinear interferometry beyond classical limit enabled by cyclic dynamics, Nat. Phys. **18**, 167 (2022).

[17] S. Colombo, E. Pedrozo-Peñafiel, A. F. Adiyatullin, Z. Li, E. Mendez, C. Shu, and V. Vuletić, Time-reversal-based quantum metrology with many-body entangled states, Nat. Phys. **18**, 925 (2022).

[18] S. Boixo, A. Datta, S. T. Flammia, A. Shaji, E. Bagan, and C. M. Caves, Quantum-limited metrology with product states, Phys. Rev. A **77**, 012317 (2008).

[19] S. Boixo, S. T. Flammia, C. M. Caves, and J. M. Geremia, Generalized Limits for Single-Parameter Quantum Estimation, Phys. Rev. Lett. **98**, 090401 (2007).

[20] S. M. Roy and S. L. Braunstein, Exponentially Enhanced Quantum Metrology, Phys. Rev. Lett. **100**, 220501 (2008).

[21] U. Khalid, J. Rehman, and H. Shin, Metrologically resourceful multipartite entanglement under quantum many-body effects, Quantum Sci. Technol. **6**, 025007 (2021).

[22] Y. Li and Z. H. Ren. Nonlocal operation enhanced entanglement detection and classification, Physica A **596**, 127137 (2022).

[23] Sudha, A. R. Usha Devi, and A. K. Rajagopal, Monogamy of quantum correlations in three-qubit pure states, Phys. Rev. A **85**, 012103 (2012).

[24] C. Schwemmer, L. Knips, M. C. Tran, A. Rosier, W. Laskowski, T. Paterek, and H. Weinfurter, Genuine Multipartite Entanglement without Multipartite Correlations, Phys. Rev. Lett. **114**, 180501 (2015).

[25] D. Das, S. Dogra, K. Dorai, and Arvind, Experimental construction of a W superposition state and its equivalence to the Greenberger-Horne-Zeilinger state under local filtration, Phys. Rev. A **92**, 022307 (2015).

[26] A. Singh, K. Dorai, and Arvind, Theoretically identifying the entanglement class of pure tripartite states, Quantum Inf. Process **17**, 334 (2018).

[27] H. Singh, Arvind, and K. Dorai, Evolution of tripartite entangled states in a decohering environment and their theoretical protection using dynamical decoupling, Phys. Rev. A **97**, 022302 (2018).

[28] E. Ising, Contribution to the theory of ferromagnetism, Z. Phys. **31**, 253 (1925).

[29] H. J. Lipkin, N. Meshkov, and A. Glick, Validity of many-body approximation methods for a solvable model: (I) Exact solutions and perturbation theory, Nucl. Phys. **62**, 188 (1965).

[30] P. M. Anisimov, G. M. Raterman, A. Chiruvelli, W. N. Plick, S. D. Huver, H. Lee, and J. P. Dowling, Quantum Metrology with Two-Mode Squeezed Vacuum: Parity Detection Beats the Heisenberg Limit, Phys. Rev. Lett. **104**, 103602 (2010).

[31] R. J. Birrittella, P. M. Alsing, and C. C. Gerry, The parity operator: Applications in quantum metrology, AVS Quantum Sci. **3**, 014701 (2021).

[32] J. S. Pratt and J. H. Eberly, Qubit cross talk and entanglement decay, Phys. Rev. B **64**, 195314 (2001).

[33] J. T. Barreiro, J. D. Bancal, P. Schindler, D. Nigg, M. Hennrich, T. Monz, N. Gisin, and R. Blatt, Demonstration of genuine multipartite entanglement with device-independent witnesses, Nat. Phys. **9**, 559 (2013).

[34] F. Dolde, V. Bergholm, Y. Wang, I. Jakobi, B. Naydenov, S. Pezzagna, J. Meijer, F. Jelezko, P. Neumann, T. Schulte-Herbrüggen, J. Biamonte, and J. Wrachtrup, High-fidelity spin entanglement using optimal control, Nat. Commun. **5**, 3371 (2014).

[35] P. Parrado-Rodríguez, C. Ryan-Anderson, A. Bermudez, and M. Müller, Crosstalk suppression for fault-tolerant quantum error correction with trapped ions, Quantum **5**, 487 (2021).

[36] Y. Li, L. Pezzè, M. Gessner, Z. Ren, W. D. Li, and A. Smerzi, Frequentist and Bayesian quantum phase estimation, Entropy **20**, 628 (2018).

[37] R. A. Fisher, Theory of statistical estimation, Math. Proc. Cambridge Philos. Soc. **22**, 700 (1925).

[38] B. Lücke, M. Scherer, J. Kruse, L. Pezzè, F. Deuretzbacher, P. Hyllus, O. Topic, J. Peise, W. Ertmer, J. Arlt, L. Santos, A. Smerzi, and C. Klempt, Twin matter waves for interferometry beyond the classical limit, Science **334**, 773 (2011).

[39] Y. Li and W. D. Li, Reasonable method to extract Fisher information from theoretical data, Physica A **514**, 606 (2019).

[40] Y. Li, L. Pezzè, W. D. Li, and A. Smerzi, Sensitivity bounds for interferometry with Ising Hamiltonians, Phys. Rev. A **99**, 022324 (2019).

[41] J. Liu, H. Yuan, X. M. Lu, and X. G. Wang, Quantum Fisher information matrix and multiparameter estimation, J. Phys. A: Math. Theor. **53**, 023001 (2020).

[42] M. Yu, Y. Liu, P. Yang, M. Gong, Q. Cao, S. Zhang, H. Liu, M. Heyl, T. Ozawa, N. Goldman, and J. Cai, Quantum Fisher information measurement and verification of the quantum Cramér-Rao bound in a solid-state qubit, npj Quantum Inf. **8**, 56 (2022).

[43] L. Pezzè, Y. Li, W. D. Li, and A. Smerzi, Witnessing entanglement without entanglement witness operators, Proc. Natl. Acad. Sci. **113**, 11459 (2016).

[44] H. J. Briegel, D. E. Browne, W. Dür, R. Raussendorf, and M. Van den Nest, Measurement-based quantum computation, Nat. Phys. **5**, 19 (2009).

[45] O. Gühne and G. Tòth, Entanglement detection, Phys. Rep. **474**, 1 (2009).

[46] N. Friis, G. Vitagliano, M. Malik, and M. Huber, Entanglement certification from theory to experiment, Nat. Rev. Phys. **1**, 72 (2019).

[47] Z. H. Ren, W. D. Li, A. Smerzi, and M. Gessner, Metrological Detection of Multipartite Entanglement from Young Diagrams, Phys. Rev. Lett. **126**, 080502 (2021).

[48] K. P. Seshadreesan, P. M. Anisimov, H. Lee, and J. P. Dowling, Parity detection achieves the Heisenberg limit in interferometry with coherent mixed with squeezed vacuum light, New J. Phys. **13**, 083026 (2011).

[49] S. Wang and J. D. Zhang, SU(1, 1) interferometry with parity measurement, J. Opt. Soc. Am. B **38**, 2687 (2021).

[50] T. Hatomura, A. Yoshinaga, Y. Matsuzaki, and M. Tatsuta, Quantum metrology based on symmetry-protected adiabatic transformation: Imperfection, finite time duration, and dephasing, New J. Phys. **24**, 033005 (2022).

[51] J. J. Bollinger, W. M. Itano, D. J. Wineland, and D. J. Heinzen, Optimal frequency measurements with maximally correlated states, Phys. Rev. A **54**, R4649 (1996).

[52] T. Monz, P. Schindler, J. T. Barreiro, M. Chwalla, D. Nigg, W. A. Coish, M. Harlander, W. Hänsel, M. Hennrich, and R. Blatt, 14-Qubit Entanglement: Creation and Coherence, Phys. Rev. Lett. **106**, 130506 (2011).

[53] D. Leibfried, M. D. Barrett, T. Schaetz, J. Britton, J. Chiaverini, W. M. Itano, J. D. Jost, C. Langer, and D. J. Wineland, Toward Heisenberg-limited spectroscopy with multiparticle entangled states, Science **304**, 1476 (2004).

[54] Z. Huang, C. Macchiavello, and L. Maccone, Usefulness of entanglement-assisted quantum metrology, Phys. Rev. A **94**, 012101 (2016).

[55] F. Ozaydin, Phase damping destroys quantum Fisher information of W states, Phys. Lett. A **378**, 3161 (2014).